Peng Gong,[1] Ivaylo H. Katzarov,[2] Anthony T. Paxton,[2] and W. Mark Rainforth[1]

[1]*Department of Materials Science and Engineering,*

University of Sheffield, Mappin Street, Sheffield, S1 3JD, UK

[2]*Department of Physics, King's College London, Strand, London, WC2R 2LS, UK*

(Dated: November 13, 2019)

Abstract

I. INTRODUCTION

II. EXPERIMENTAL

Mark, Peng, you can start typing here...

III. THEORETICAL

A. Introduction and background

At the heart of the simulation of hydrogen effects on plasticity is the model that is used to describe the connection between background, or nominal, hydrogen concentration, $C_{\rm H}$, here defined in units of atomic parts per million, appm; and either the flow stress or the average dislocation velocity, $\bar{v}_{\rm dis}$. At the simplest level as used in typical discrete dislocation dynamics simulations or crystal plasticity finite element models, simple ad hoc assumptions are used [1, 2]. However, $\bar{v}_{\rm dis}$ is a complex function of $C_{\rm H}$, and depending on applied stress and temperature $\bar{v}_{\rm dis}$ can be both *enhanced* and *reduced* depending on the background hydrogen concentration [3]. In earlier work [3, 4], two of us developed an off-lattice kinetic Monte-Carlo method to calculate the velocity of screw dislocations in α-Fe based upon first principles calculations of kink-pair formation energies [5]. In this model a number of quite serious approximations are made, namely, (*i*) the kink pair formation energy is affected only by hydrogen ahead of the dislocation in the glide plane; (*ii*) kink velocity is only affected by hydrogen behind the dislocation in the glide plane; (*iii*) hydrogen is assumed to remain fixed in place during kink-pair formation and migration; (*iv*) the time for segments of dislocation to move between Peierls valleys is assumed greater than the hydrogen jump time within the dislocation core. In spite of its simplicity that model was able to predict dislocation velocity as a function of temperature, stress, τ, and nominal hydrogen concentration and it was shown that such a function is non monotonic and that the effect of hydrogen can be to increase or decrease dislocation velocity, depending on conditions; and that the change in velocity compared to pure α-Fe at 300K and $\tau = 100$ MPa increases by more than a factor of 10 up to 5 appm and then decreases to less than the velocity in pure α-Fe at 20 appm. In addition, the simulations [3] *predicted* that under most conditions of hydrogen-loaded α-Fe a moving screw dislocation will leave a trail of debris made up of rows of prismatic loops. The

central result of the present paper is that *we have found these loops* in electron microscope images of deformed, hydrogen-charged α-Fe. On the other hand the model was not able to reproduce activation volume measurements [6] which indicate a minimum in the dislocation velocity as a function of hydrogen concentration at about 10 appm at 300K. We present here a new model which we call "self consistent kinetic Monte-Carlo" (SCkMC) which permits a dynamic non equilibrium distribution of hydrogen about the moving dislocation core. Specific new features of the model are, (*i*) simultaneous kink nucleation, migration and hydrogen jumping; (*ii*) kink pair formation energy affected by all hydrogen within the core; (*iii*) a non equilibrium distribution of hydrogen which depends on temperature and average dislocation velocity; (*iv*) kink pair formation energy depends on average dislocation velocity; (*v*) mobile hydrogen during glide—although the *total* hydrogen occupancy within the core is assumed fixed.

B. Line tension model

The SCkMC is predicated on a parameterised line tension model [5, 7]. We imagine a long dislocation lying in its Peierls valley, a segment of which has migrated towards or into the next Peierls valley so as to make an incipient or complete kink pair. The dislocation is divided into bins of width b, the Burgers vector, along its length and a variable x_j is assigned to describe the deviation of the segment lying in the j^{th} bin from the dislocation's original position in the Peierls valley—the elastic center of the dislocation. There is a periodic Peierls energy landscape described by an energy function, $E_p\left(x_j\right)$. The energy per unit length of dislocation is then prescribed in the following line tension expression [5],

$$\begin{aligned} E &= \sum_j E_j \\ &= \frac{1}{2}K\sum_j \left(x_j - x_{j+1}\right)^2 + \sum_j E_p\left(x_j\right) + \sum_j \epsilon_{1pq}\tau_{pr}b_r\xi_p x_j - \sum_{jk} E_{\text{H}}\left(\left|x_j - x_k^{\text{H}}\right|\right) \end{aligned} \tag{1}$$

The first term describes the energy penalty for two bins which have different amounts of deviation from the original Peierls valley towards the next and K is the associated "spring constant". The second term is the energy of the segment j depending on its height in the Peierls landscape. The third term, with an implicit sum from 1 to 3 over $\{pqr\}$, is the 1-component (perpendicular to [111]) of the Peach–Kohler force arising from a local stress

τ_{pq} times the displacement of the j^{th} segment of dislocation having a line sense $\boldsymbol{\xi}$. This term "tilts" the corrugated energy landscape so that the Peierls valley ahead of the dislocation is lower in energy that the one behind, and provides the driving force for glide. The final term expresses the energy associated with a hydrogen atom that is trapped at a position at a distance $|x_j - x_k^{\text{H}}|$ from the core, in which x_k^{H} is the position of the k^{th} hydrogen atom relative to the elastic centre.

C. Dynamics of the long straight dislocation

We first examine the motion of a long straight dislocation, its line moving as a whole. And in the next section we address the actual situation of glide by the Peierls mechanism of kink pair creation and kink migration [8]. Density functional theory (DFT) calculations have identified two core structures of the $\frac{1}{2}\langle 111\rangle$ screw dislocation, the so called "easy core" (EC), which is the stable, low energy configuration, and the "hard core" (HC) which is metastable [7, 9]. The HC is very close in configuration to the "saddle point" (SP) core [7, 9]. DFT calculations furthermore show that hydrogen binds strongly to the EC with three equivalent sites having binding energies of $E_i = 256$ meV in the so called E_1/E_2 basin, three in the E_3/E_4 basin having $E_i = 201$ meV and six in the E_7/E_8 basin with $E_i = 77$ meV [5]. The strongest binding sites for the HC are one in the H_0/H_1 basin located at the centre of the core with $E_i = 390$ meV, and six binding sites denoted H_2 having $E_i = 189$ meV [5]. As a dislocation moves from EC to HC to EC hydrogen in the E_1/E_2 traps sites ahead of the dislocation line transform into H_0/H_1 sites and finally the hydrogen occupies E_1/E_2 traps sites behind the dislocation line.

When the dislocation is lying in its equilibrium Peierls valley the probability of occupancy of a trap site, i, is determined by the McClean isotherm,

$$\chi_i = \frac{\frac{1}{6}C_0\, e^{E_i/kT}}{1 + \frac{1}{6}C_0\, e^{E_i/kT}} \tag{2}$$

in which $C_0 = 10^{-6}C_{\text{H}}$ is the nominal number of hydrogen atoms per Fe atom, and the factor 1/6 accounts for there being six tetrahedral sites per bulk Fe atom. Here, k is the Boltzmann constant and T is the absolute temperature. If we take a sum over all the trap sites in the dislocation core, we will define

$$\chi_t = \sum_i \chi_i = \text{constant} \tag{3}$$

as the total hydrogen occupancy of the core sites; and we will assume throughout that *this is constant*, that is, hydrogen will redistribute dynamically between trap sites during glide but overall the dislocation will not absorb or reject hydrogen; we also only allow hydrogen to redistribute among traps within a plane perpendicular to the dislocation line, in view of the very slow hydrogen pipe diffusivity [10]. In the case of slow glide, and the maintenance of equilibrium, then as a long straight dislocation moves between two Peierls valleys, we may define the occupation probability of trap site i as [11],

$$\chi_i^{\mathrm{e}}(x) = \frac{\chi_t e^{-E_i(x)/kT}}{\sum_j e^{-E_i(x)/kT}} \tag{4}$$

Here $0 < x < h$, if $h = a\sqrt{2/3} = 2.34$ Å is the period of the Peierls potential on the $(\bar{1}10)$ plane, so that x describes the position of the dislocation line with respect an origin at the EC elastic centre. As the dislocation glides hydrogen will redistribute between trap sites, which themselves distort and therefore whose trap depth, $E_i(x)$, varies with x. We parameterise $E_i(x)$ by fitting and interpolation of DFT data [5]. Once that is done, then in association with the line tension model (1) we have a complete description of the energetics of the dislocation as a function of x and the total occupancy, χ_t, *for the moment only* in two limiting cases: (a) equilibrium, slow glide in which traps are occupied according to (4), and (b) fast glide, in which all hydrogen atoms are fixed in the traps they occupy in the EC initial state before glide.

(a) Fig. 1(a) shows potential energy profiles in the equilibrium limit of a slowly moving dislocation. At $C_{\mathrm{H}} = 0$ the profile is typical of a calculated Peierls barrier [12]. The Peierls barrier shown predicted by our model is consistent with the measured estimate of 37 meV/b [8]. The barrier becomes smaller as C_{H} is increased because hydrogen is stablising the saddle point core as the $E1/E2$ traps distort into $H0/H1$ traps. In fact the effect is strong enough so that when C_{H} exceeds 30 appm the saddle point core is lower in energy than the easy core and their roles are reversed; this is because the total energy gained by hydrogen in deeper traps overwhelms the penalty in core energy. In this way the Peierls barrier is reduced to close to zero and then increases again. However above about 30 appm hydrogen the saddle point is at the EC, and the minimum is in the HC configuration.

(b) In the limit of *rapid glide* the hydrogen atoms are kept fixed during the movement of a dislocation between Peierls valleys then as the dislocation moves, hydrogen that was

trapped in deep traps may not jump into the newly created traps, but instead remains behind in sites of higher potential energy; hence the Peierls barrier increases continually with $C_{\rm H}$ and the initial and final positions of the dislocation line have not the same energy: the profile is asymmetric as shown in Fig. 1(b).

FIG. 1. Peierls potential: the potential energy in units of eV per Burgers vector of a long straight $\frac{1}{2}\langle 111\rangle$ screw dislocation as a function of distance between one Peierls valley and the next. (a) Limiting case of slow motion: the hydrogen remains in equilibrium and moves reversibly between E_1/E_2 basins. At the saddle point the hydrogen is trapped at the H_0/H_1 basin near the saddle point. Note, how as hydrogen concentration is increased above 30 appm the saddle point core structure becomes more stable than the easy core. (b) Limiting case of high dislocation velocity: the hydrogen remains behind in a trap site of high energy compared to the E_1/E_2 basin hence the line tension is greater after glide by one repeat distance than before. The curves are labelled with the nominal background hydrogen concentration, $C_{\rm H}$. Temperature is 300K.

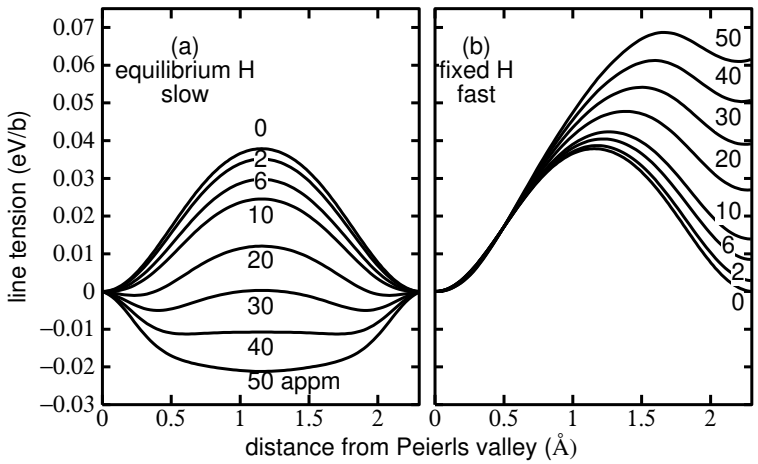

A highly relevant conclusion is that trapped hydrogen serves to *stabilise the hard core with respect to the easy core*, so that hydrogen is able to trigger a core transformation which strongly modifies the Peierls barrier.

The results in Fig. 1 suggest to us that the actual profile will be somewhere in between the two limits, the departure from equilibrium being controlled by the uniform dislocation velocity, v. Therefore we seek a theory that will predict the profile as a function of v. Because of the finite speed of the dislocation, we expect that the probability of occupancy of trap i, $\chi_i(x)$ differs from its equilibrium value (4), $\chi_i^{\rm e}(x)$. For any of the 10 strongest

binding sites we find the following continuity equation,

$$\frac{\partial \chi_i(x,v)}{\partial t} = v\,\frac{\partial \chi_i(x,v)}{\partial x} = \left(\chi_i^{\mathrm{e}}(x) - \chi_i(x,v)\right)\,\nu\,\mathrm{e}^{-E_i(r)/kT} \tag{5}$$

where ν is an "attempt frequency" for hydrogen to escape from the i^{th} trap [13]. By solving (5), subject to the condition (3) that the total hydrogen occupancy remains constant, we may determine the potential energy of the dislocation as a function of position between two Peierls valleys at velocity, v. We show these data in Fig. 2.

FIG. 2. Potential energy of a long straight $\frac{1}{2}\langle 111\rangle$ screw dislocation as in Fig. 1. Panels (a), (b) and (c) show solutions using the continuity equation (5) at nominal hydrogen concentrations of 10, 30 and 50 appm respectively. In cases where the saddle point is of lower energy than the EC end points, the Peierls barrier is inferred by taking the end points as saddle point energies and the stable core to be the HC. Curves for dislocation velocities, v, between 5×10^4 and 3×10^{10} nm s^{-1} are shown. Temperature is 300K.

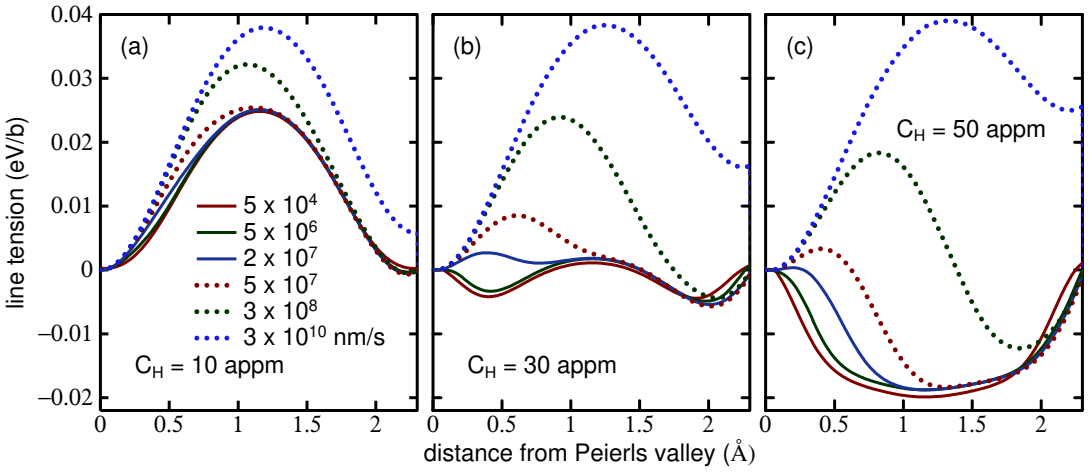

We observe that at the critical C_{H} of 30 appm where the Peierls barrier for low velocity is close to zero, the actual barrier is strongly dependent on the velocity and only vanishes in the slow, equilibrium limit.

D. Dynamics by kink pair creation and migration

The $\frac{1}{2}\langle 111\rangle$ screw dislocation in bcc transition metals is characterised by its non planar, non degenerate core structure [14] which means that even at the lowest temperatures, its glide is via a *Peierls mechanism*, namely the process of kink pair creation followed by kink

migration [11]. Kink pair generation is thermally activated. We therefore turn now to the actual problem of predicting $\bar{v}_{\rm dis}$ within the Peierls mechanism [8].

1. Kink pair creation

The screw dislocation does not lie quiescent in its Peierls valley; fluctuations produce random events in which a small section deviates towards a neighbouring Peierls valley. Mostly this produces an "incipient" kink pair which annihilates due to elastic attraction of the kinks. A stable kink pair is one that has sufficient distance between the kinks, which we take to be about $30b$ [3, 7], that elastic attraction is small enough to allow the kink pair to survive and its halves to separate under the local stresses they encounter. The formation of a stable kink pair is a result of numerous acts of kink-pair nucleation, annihilation, and increasing distance between kinks under the action of the applied shear stress. We do not consider all these processes explicitly in our simulations. The rare event of formation of a stable kink pair, which separates under the resolved shear stress is treated using the kinetic Monte-Carlo procedure described elsewhere [3, 15, 16].

The reason for requiring a *self consistent* theory is that trapped hydrogen will strongly modify the kink pair formation enthalpy, $E_{\rm kp}$, and that the location of hydrogen in traps will depend on how fast the dislocation is moving. Hence $E_{\rm kp}$ is a function of $\bar{v}_{\rm dis}$ since it depends on the rate at which hydrogen is distributed among trap sites as the dislocation glides. For a given resolved shear stress, τ, and an assumed average velocity, $\bar{v}_{\rm dis}$, using the line tension model and data such as in Fig 2 the energy, $E(C_{\rm H}, x, \bar{v}_{\rm dis})$, of a dislocation segment, Eq. (1), of length b and at a distance x from the EC elastic centre in the initial Peierls valley, can be calculated. Then using linear, non-singular elastic theory [11, 16] and the "nudged elastic band" (NEB) method [17], we may calculate the kink pair formation enthalpy, $E_{\rm kp}(C_{\rm H}, \tau, \bar{v}_{\rm dis})$. *Howeve*r $E_{\rm kp}$ is a function of $\bar{v}_{\rm dis}$ while $\bar{v}_{\rm dis}$ is a function of $E_{\rm kp}$: $E_{\rm kp} = E_{\rm kp}(\bar{v}_{\rm dis})$ and $\bar{v}_{\rm dis} = \bar{v}_{\rm dis}(E_{\rm kp})$. To make progress and to find a self consistent solution, we assume that the average speed is constant, and

$$\bar{v}_{\rm dis}(E_{\rm kp}) = \frac{h}{t_r} \tag{6}$$

allowing us to define an *average relaxation time* for kink pair formation,

$$t_r = \nu_{\rm kp}^{-1} {\rm e}^{E_{\rm kp}(C_{\rm H},\tau,v)/kT} \tag{7}$$

where ν_{kp} is an attempt frequency for which we use the Debye frequency of α-Fe. In order to solve (6) and (7), and to determine E_{kp} at given C_{H} and τ, we proceed with the following iterative process.

1. Assume an initial E_{kp}.

2. Calculate the corresponding $\bar{v}_{\mathrm{dis}}$ using (6) and (7).

3. Determine the distribution of hydrogen from the continuity equation (5), subject to (3); and calculate the segment energy, $E(C_{\mathrm{H}}, x, \bar{v}_{\mathrm{dis}})$ from the line tension model.

4. Calculate E_{kp} using the NEB and go to step 2.

This process is iterated until E_{kp} calculated in step 4 is no longer changing to within some tolerance. Figure 3 shows the results of the iterative procedure.

FIG. 3. Kink pair formation enthalpy, E_{kp}, as a function of resolved shear stress, τ and average dislocation velocity, $\bar{v}_{\mathrm{dis}}$; calculated by iterative solution of equations (6) and (7).

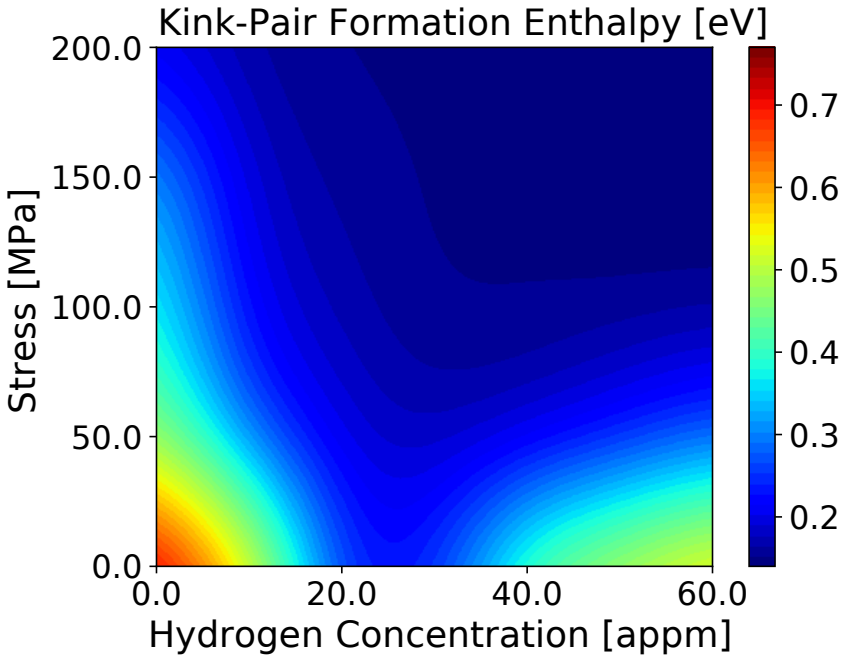

We may interpret Fig. 3 in the following way. At high stress, E_{kp} is uniformly small because the applied stress acts to drive a dislocation into the next Peierls valley and this dominates the process of glide. At low stress we observe a large E_{kp} at low C_{H}, the largest being that of pure α-Fe and zero stress. As C_{H} increases, E_{kp} decreases, consistent with the calculations shown in Fig. 1. E_{kp} reaches a minimum at $C_{\mathrm{H}} \approx 30$ appm in Fig. 3 as predicted in Fig. 1 and this minimum in E_{kp} is a consequence of the hydrogen-induced core transformation from EC to HC. As C_{H} increases further E_{kp} rises as a consequence of the

increasing Peierls barrier—but now the barrier is at the easy core configuration and the Peierls valley corresponds to the HC.

2. Kink migration

Glide is a two step process. After the formation of a stable double kink the two kinks will separate in opposite directions. In pure metal, the kink migration or *secondary Peierls barrier* is low and is not thermally activated. However hydrogen and other interstitials change that. If a hydrogen atom is trapped in the $E1/E2$ basin just behind the dislocation line and a kink sweeps past, then that hydrogen ends up in a higher enthalpy trap site [5], which implies that thermal activation is then required for the kink to proceed. We do not need to rehearse the kMC procedure here since we use the identical scheme as described earlier [3]. However we should underline the *physics* here since it is essential in appreciating the present findings. In the case of pure α-Fe, a screw dislocation of typical length of about $1000b$ will glide as a unit as in face centred cubic metals (albeit by thermal activation of kink pairs) since the kink migration speed is so fast that a kink pair has separated to the ends of the dislocation before the next kink pair is activated [3]. Hence kink collision does not occur. The situation is very different if the kinks suffer solute drag due to hydrogen and other interstitials. A key fact is that kink pairs are created on any one of the three $\{\bar{1}10\}$ glide planes in the zone of the [111] Burgers vector. *If two kinks on different glide planes collide* the resulting defect is an edge jog which is sessile. Our findings earlier [3], which we confirm here, are that such jogs amount to self pinning points which drag out edge dipoles and these dipoles will pinch out to create a train of prismatic loop debris, *entirely as a consequence of dissolved hydrogen.*

E. Results of the self consistent kinetic Monte-Carlo simulations

1. Average dislocation velocity

Conditions of the present self consistent kMC simulations are identical to those of the earlier non self consistent modelling [3]. Temperature is 300K. Rather than using a kink pair formation energy that depends only on stress, C_{H} and temperature; we now employ

E_{kp} as a function of $\bar{v}_{\mathrm{dis}}$ also as taken from Fig 3. Average dislocation velocity as a function of stress and C_{H} is shown in Fig. 4.

FIG. 4. Average dislocation velocity calculated within the self consistent kinetic Monte-Carlo model using E_{kp} from Fig. 3.

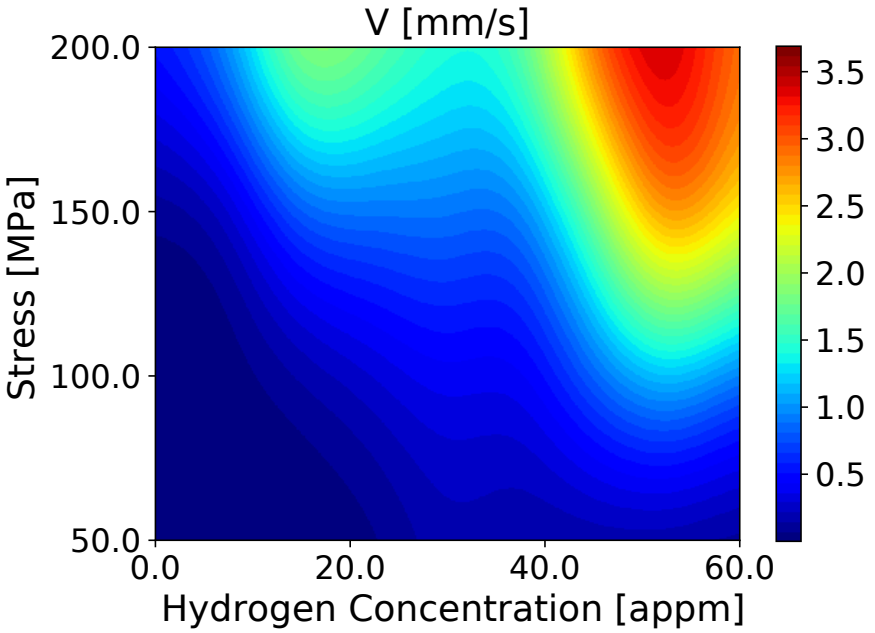

For $\tau < 50$ MPa (not shown in Fig. 4), $\bar{v}_{\mathrm{dis}}$ increases with C_{H}, reaching a maximum at $C_{\mathrm{H}} \approx 25$ appm; thereafter $\bar{v}_{\mathrm{dis}}$ decreases as a result of the increase in E_{kp} (Fig. 3). At $\tau > 100$ MPa, $\bar{v}_{\mathrm{dis}}$ does not go through a minimum, but increases steadily with C_{H} until $C_{\mathrm{H}} \approx 40$ appm at which a rather dramatic increase is found, followed by a decline at higher hydrogen concentrations. The greatest average dislocation velocity, for all stresses, occurs at a nominal hydrogen concentration of about 50 appm. This complex behaviour can be traced in part to the concentration dependence of the kink pair formation enthalpy and the hydrogen-induced core transition from easy core to hard core. If E_{kp} is small or vanishing then kink pair formation is easy on all three glide planes in the zone of the Burgers vector, and this leads to increased likelihood of kink pair collisions on different glide planes. Once an immobile jog is created further kinks pile into it, resulting in the formation of superjogs and trailing dislocation dipoles. The two arms of the dipole may intersect and recombine by kink pair recombination. Thereby the dipole is unzipped and a straight dislocation in screw orientation is restored. This involved set of operations serves greatly to attenuate the average dislocation velocity as the overall line waits for these events to complete and the

dislocation to unpin itself.

2. The development of debris

FIG. 5. Snapshots of a moving $\frac{1}{2}[111]$ screw dislocation (black line) projected onto $(\bar{1}10)$ (upper line) and $(11\bar{2})$ (lower line) planes. The red lines indicate trailing debris. Blue dots represent the positions of hydrogen atoms. $\tau = 100$ MPa, $T = 300$K (a) $C_{\rm H} = 0$, (b) $C_{\rm H} = 10$ appm, (c) $C_{\rm H} = 30$ appm, (d) $C_{\rm H} = 50$ appm

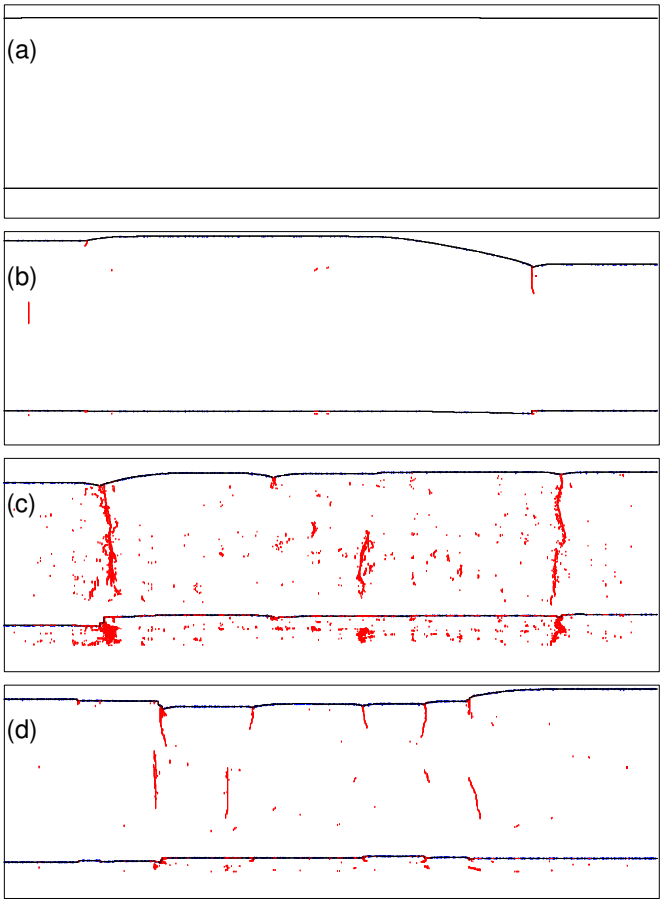

These observations are illustrated in Fig. 5 which show simulations at a resolved shear stress, $\tau = 100$ MPa, and $T = 300$K. In each panel the upper black line shows a snapshot of a moving $\frac{1}{2}[111]$ screw dislocation projected onto the primary $(\bar{1}10)$ glide plane, while the lower black line shows the *same* dislocation at the same time projected onto the perpendicular $(11\bar{2})$ plane. This second projection serves to indicate the extent to which the dislocation deviates from its primary glide plane into the two cross slip planes in the [111] zone.

(a) At $C_{\rm H} = 0$, panel (a) illustrates the point made earlier that kink velocity is high and the dislocation moves as a straight line (although at $T = 400$K kink pair generation is sufficiently frequent that kink collisions do occur and some debris is observed [3]).

(b) At $C_{\rm H} = 10$ appm, Fig 5(b), $E_{\rm kp}$ is large (Fig. 3) and nucleation on cross slip planes is rare so that kink collisions on different slip planes is less likely—some debris is seen and the dislocation is not straight in its primary slip plane, however deviation onto a cross slip plane is limited.

(c) At $C_{\rm H} = 30$ appm $E_{\rm kp}$ is small (Fig. 3) and nucleation on cross slip planes is commonplace: there is much debris observed and significant cross slip of the dislocation onto secondary glide planes.

(d) As $C_{\rm H}$ is further raised to 50 appm, Fig 5(d), $E_{\rm kp}$ is raised again (Fig. 3), the equilibrium core structure is the hard core and kink pair generation on the cross slip planes is again less common—less debris accumulates than at $C_{\rm H} = 30$ appm.

3. The "30 appm anomaly" and comparison with experiment

FIG. 6. Calculated dislocation velocity, $\bar{v}_{\rm dis}$, averaged over resolved shear stresses in the interval 50–200 MPa

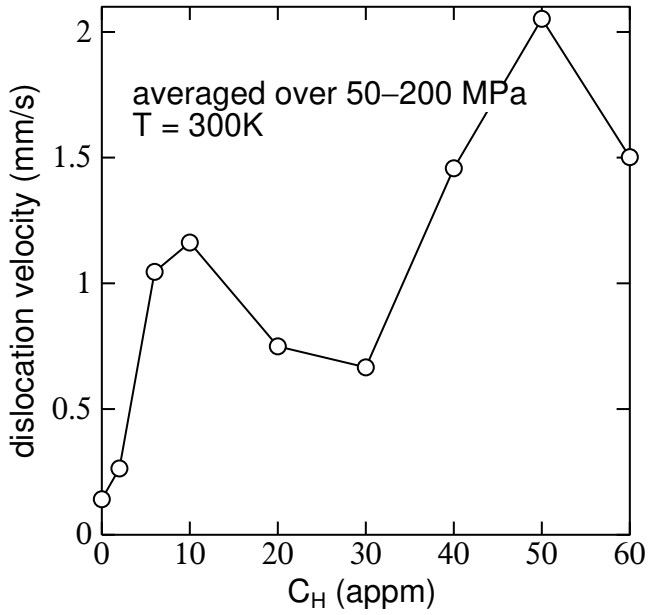

It is very clear from all the results presented above that there is a strong non monotonic dependence of $\bar{v}_{\rm dis}$ on $C_{\rm H}$ with an "anomaly" occurring around $C_{\rm H} = 30$ appm. The reason for

this is the reduction in kink pair formation enthalpy and the associated core transformation from EC to HC. This effect is revealed most simply in Fig. 6 which is a plot of $\bar{v}_{\rm dis}$ averaged over resolved shear stresses in the interval 50–200 MPa. This evident dip in $\bar{v}_{\rm dis}$ is mirrored in measurements of the components of the activation volume for tensile deformation of hydrogen charged α-Fe. The method used is stress relaxation [18]. The applied shear stress is divided into a thermally activated contribution, $\tau_{\rm eff}$, and a term, τ_μ, that depends on temperature only through the T-dependence of the shear modulus [19],

$$\tau_{\rm app} = \tau_\mu + \tau_{\rm eff}$$

The strain rate as a function of temperature is given in terms of an activation free energy, G, of the strain rate, $\dot{\gamma}$, defined through,

$$\dot{\gamma} = \dot{\gamma}_0 \, e^{-G/kT}$$

where $\dot{\gamma}_0$ is given by the Orowan equation [18] and depends on the average dislocation velocity. The "effective" activation volume is

$$V_{\rm eff} = -\frac{{\rm d}G}{{\rm d}\tau_{\rm eff}}$$

What is measured is the consequence of the total applied shear stress, namely an "apparent" activation volume,

$$V_{\rm app} = V_{\rm eff}\left(1 + S'\frac{{\rm d}\tau_\mu}{{\rm d}\gamma}\right) = V_{\rm eff} + V_{\rm h}$$

where S' is the compliance of the specimen plus loading train in the tensometer. Stress relaxation tests allow the two terms, the effective and the "hardening" activation volumes to be identified separately. Fig. 7 shows such measurements, taken from Ref. [6]. Hydrogen concentration is difficult to measure and coupled with uncertainties in our parameterisation of the SCkMC, there is a factor of two discrepancy between theory and experiment in the $C_{\rm H}$ value where the anomaly occurs.

FIG. 7. Measured components of the activation volume for plastic shear in hydrogen loaded pure α-Fe. After Ref. [6]

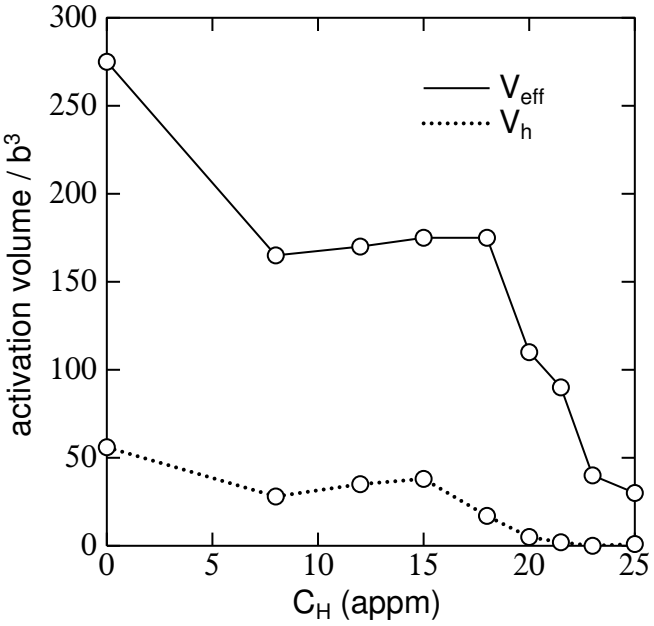

4. Implication for development of cellular dislocation structure and sub-grain boundaries

Transmission electron microscopy (TEM) observations of dislocation structures of hydrogencharged specimens in α-Fe show that the homogeneous dislocation forest existing in hydrogenfree samples transforms into cell walls that separate relatively dislocation free regions [6]. The cell walls can be regarded as dense dislocation tangles. The driving force for cell wall formation arises from the reduction in the total elastic energy of the dislocations due to their clustering. TEM images reveal that the volume of the dislocation free zones and the density of the tangled structures increase with increasing C_{H} in the interval 0–25 appm [6]. The physics that lies behind dislocation reorganisation due to hydrogen is not yet well understood. It has been commonly accepted that a requirement for cell formation is that dislocations have sufficient mobility out of their slip plane [20]. Therefore, whether cells form or not depends on factors which determine the ease with which dislocations cross slip or climb. The present SCkMC simulations show that the probability for formation of kink pairs in secondary slip planes and dislocation segments which glide out of the primary slip plane increases with C_{H}. The angle describing the deviation of the dislocation from the primary slip plane as a function of applied stress and C_{H} is shown in Fig. 8. Again,

at moderate stresses where glide is dominated by kink pair formation enthalpy, we see an anomaly near $C_{\mathrm{H}} = 30$ appm near the EC–HC core transformation, where E_{kp} is small and kink pair activation is prolific on the cross slip planes. SCkMC simulations show that the dislocation mobility out of the primary slip plane increases significantly for $C_{\mathrm{H}} > 10$ appm and applied stresses higher than 100 MPa. This result of the SCkMC simulations agrees with TEM observations indicating an increase of the density of the tangled structures with increase of hydrogen concentration.

FIG. 8. The angle describing the deviation of a long straight $\frac{1}{2}\langle 111\rangle$ screw dislocation from the primary glide plane, after moving over a distance of 50 nm, as a function of C_{H} and resolved shear stresses.

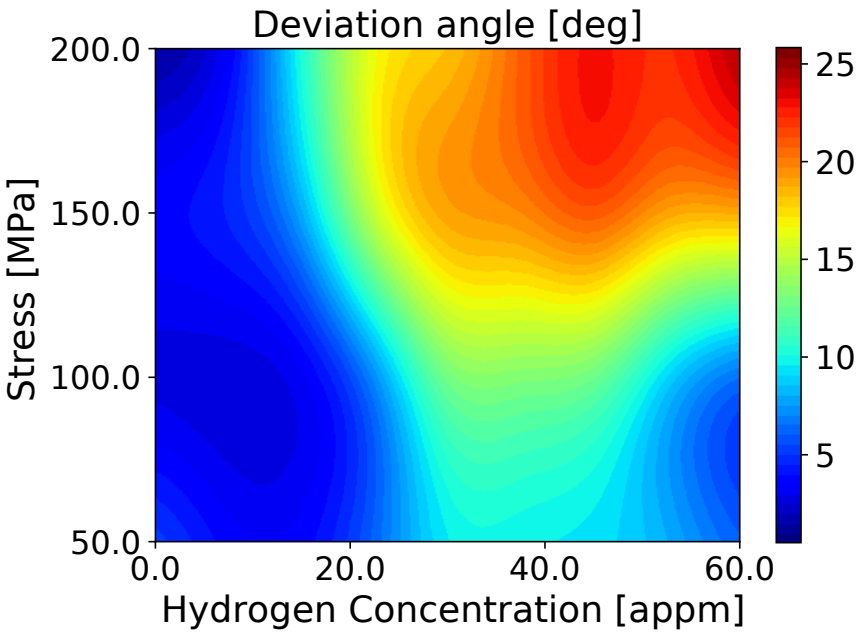

It is a matter of further work to investigate the role of hydrogen and other interstitials such as carbon on the dynamics of cell formation and the development of cellular and sub-grain microstructures.

[1] Barera, O. & Cocks, A. C. F. Computational modelling of hydrogen embrittlement in welded structures. *Philosophical Magazine* **93**, 2680–2700 (2013).

[2] Castelluccio, G. M., Geller, C. B. & McDowell, D. L. A rationale for modeling hydrogen effects on plastic deformation across scales in FCC metals. *Int. J. Plasticity* **111**, 72–84 (2018).

[3] Katzarov, I. H., Pashov, D. L. & Paxton, A. T. Hydrogen embrittlement I. Analysis of hydrogen-enhanced localized plasticity: Effect of hydrogen on the velocity of screw dislocations in α-Fe. *Phys. Rev. Materials* **1**, 033602 (2017).

[4] There was an error in Ref [3]. We employed a factor 1/3 rather than the correct factor 1/6 in the McLean isotherm (2). This means that all values of C_{H} both in the text and in the figures should be multiplied by two to be corrected.

[5] Itakura, M., Kaburaki, H., Yamaguchi, M. & Okita, T. The effect of hydrogen atoms on the screw dislocation mobility in bcc iron: A first-principles study. *Acta Materialia* **61**, 6857–6867 (2013).

[6] Wang, S., Hashimoto, N. & Ohnuki, S. Effects of hydrogen on activation volume and density of mobile dislocations in iron-based alloy. *Mat. Sci. Eng: A* **562**, 101–108 (2013).

[7] Itakura, M., Kaburaki, H. & Yamaguchi, M. First-principles study on the mobility of screw dislocations in bcc iron. *Acta Materialia* **60**, 3698–3710 (2012).

[8] Caillard, D. Kinetics of dislocations in pure Fe. Part I. In situ straining experiments at room temperature. *Acta Materialia* **58**, 3493–3503 (2010).

[9] Clouet, E., Ventelon, L. & Willaime, F. Dislocation core energies and core fields from first principles. *Phys. Rev. Letters.* **102**, 055502 (2009).

[10] Bombac, D., Katzarov, I. H., Pashov, D. L. & Paxton, A. T. Theoretical evaluation of the role of crystal defects on local equilibrium and effective diffusivity of hydrogen in iron. *Mat. Sci. Technol.* **33**, 1505–1514 (2017).

[11] Hirth, J. P. & Lothe, J. *Theory of Dislocations* (McGraw-Hil Book Company, New York, 1968), 1 edn.

[12] Mrovec, M., Nguyen-Manh, D., Elsässer, C. & Gumbsch, P. Magnetic bond-order potential for iron. *Phys. Rev. Letters* **106**, 246402 (2011).

[13] Paxton, A. T. & Katzarov, I. H. Quantum and isotope effects on hydrogen diffusion, trapping and escape in iron. *Acta Materialia* **103**, 71–76 (2016).

[14] Gröger, R., Bailey, A. G. & Vitek, V. Multiscale modeling of plastic deformation of molybdenum and tungsten: I. Atomistic studies of the core structure and glide of $\frac{1}{2}\langle 111\rangle$ screw dislocations at 0K. *Acta Materialia* **56**, 5401–5411 (2008).

[15] Deo, C. S., Srolovitz, D. J., Cai, W. & Bulatov, V. V. Stochastic simulation of dislocation glide in tantalum and Ta-based alloys. *J. Mech. Phys. Solids* **53**, 1223–1247 (2005).

[16] Bulatov, V. & Cai, W. *Computer Simulation of Dislocations* (Oxford University Press, Oxford, 2006), 1 edn.

[17] Henkelman, G. & Jónsson, H. Improved tangent estimate in the nudged elastic band method for finding minimum energy paths and saddle points. *J. Chem. Phys.* **113**, 9978–9985 (2000).

[18] Spätig, P., Bonneville, J. & Martin, J. A new method for activation volume measurements: application to Ni_3(Al,Hf). *Mat. Sci. Eng: A* **167**, 73–79 (1993).

[19] Seeger, A., Diehl, J., Mader, S. & Rebstock, H. Work-hardening and work-softening of face-centred cubic metal crystals. *Phil. Mag.* **2**, 323–350 (1957).

[20] Hirth, J. P. In Rassweiler, G. M. & Grube, W. L. (eds.) *Internal stresses and fatigue in metals*, 138 (Elsevier, New York, 1959).